TISSUE ENGINEERING: Part A
Volume 21, Numbers 11 and 12, 2015
DOI: 10.1089/ten.tea.2014.0671

New Self-Assembling Multifunctional Templates for the Biofabrication and Controlled Self-Release of Cultured Tissue

Ricardo M. Gouveia, PhD,[1] Valeria Castelletto, PhD,[2] Ian W. Hamley, PhD,[2] and Che J. Connon, PhD[1]

The need to source live human tissues for research and clinical applications has been a major driving force for the development of new biomaterials. Ideally, these should elicit the formation of scaffold-free tissues with native-like structure and composition. In this study, we describe a biologically interactive coating that combines the fabrication and subsequent self-release of live purposeful tissues using template–cell–environment feedback. This smart coating was formed from a self-assembling peptide amphiphile comprising a protease-cleavable sequence contiguous with a cell attachment and signaling motif. This multifunctional material was subsequently used not only to instruct human corneal or skin fibroblasts to adhere and deposit discreet multiple layers of native extracellular matrix but also to govern their own self-directed release from the template solely through the action of endogenous metalloproteases. Tissues recovered through this physiologically relevant process were carrier-free and structurally and phenotypically equivalent to their natural counterparts. This technology contributes to a new paradigm in regenerative medicine, whereby materials are able to actively direct and respond to cell behavior. The novel application of such materials as a coating capable of directing the formation and detachment of complex tissues solely under physiological conditions can have broad use for fundamental research and in future cell and tissue therapies.

Introduction

One of the main challenges in tissue engineering is the creation of a suitable environment, in which donor-derived cells (such as stem cells) can be seeded, grown, and induced to differentiate as they do *in vivo* toward the formation of a complex tissue.[1–3] This environment must be suitable for proper cell attachment and/or migration, allow nutrient and metabolite diffusion, and present adequate biochemical and mechanical cues. There are numerous examples in the literature and in the clinic of artificial environments that provide such a milieu of factors and conditions,[4–6] including smart or intelligent scaffolds that respond to cells with culture progression.[7–9] Some of these scaffolds were developed using fully synthetic materials to mimic the scale and chemistry of the natural extracellular matrix (ECM).[10–12] Peptide amphiphiles (PAs) constitute a notable example of such synthetic materials.[13–16] These molecules have been used for their ability to self-assemble in aqueous medium at physiological pH into highly ordered nanostructures presenting specific peptide motifs at their hydrophilic external surface, which then have the ability to interact with cultured cells and initiate downstream signaling cascades that regulate phenotype and ECM production (as extensively reviewed in Refs.[17–19]).

Recently, several alternative scaffold-free technologies have been developed to create suitable artificial environments able to instruct cells toward creating their own tissue *de novo*.[20] In this context, thermo-, electro-, photo-, and pH-responsive materials have been developed to allow an easier detachment of cells and tissues from the underlying template.[21] This bottom-up strategy is evidently attractive as it provides cells with a template to fabricate native-like tissue constructs containing an ECM resembling that of the natural organ without the need of scaffolds or carriers. In addition, by recapitulating differentiation and organogenesis *in vitro* with patient-derived cells, these methods constitute an expedient alternative source of autologous tissue for clinical applications.[22] These techniques have been used mainly to create cell sheets,[23] with limited control on the tissues'

[1]Institute of Genetic Medicine, Newcastle University, Newcastle upon Tyne, United Kingdom.
[2]School of Chemistry, Food and Pharmacy, University of Reading, Reading, United Kingdom.

© R.M. Gouveia et al. 2015; Published by Mary Ann Liebert, Inc. This Open Access article is distributed under the terms of the Creative Commons Attribution Noncommercial License (http://creativecommons.org/licenses/by-nc/4.0/) which permits any noncommercial use, distribution, and reproduction in any medium, provided the original author(s) and the source are credited.

three-dimensional structure and hierarchical organization, and using nonphysiological triggers to induce detachment. Furthermore, biologically interactive implants are gaining considerable interest within the materials science community. Thus, new methodologies are required that can be easily incorporated into future transplantable medical devices capable of directing cell and tissue formation and self-regulated therapeutic release in physiological conditions.

To begin to address these challenges, we recently characterized several self-assembling PAs carrying biofunctional motifs[24–26] shown to promote cell adhesion, proliferation, and survival while enhancing stratification and controlling the orientation of subsequent ECM deposition.[27] This has led to the present study, where we developed a bottom-up strategy to create scaffold-free bioprosthetic tissues with native-type structure and composition and under fully defined physiological conditions. To this end, we developed a novel, fully synthetic multifunctional PA ($_{mf}$PA) comprising a hydrophobic C_{16} aliphatic chain linked to a relatively hydrophilic peptide sequence of 14 amino acids (Fig. 1a). This peptide head was designed to perform as a multipurpose biofunctional cue comprising two contiguous bioactive motifs, both derived from natural proteins. The N-terminal sequence Thr-Pro-Gly-Pro-Gln-Gly-Ile-Ala-Gly-Gln (TPGPQGIAGQ) was derived from the matrix metalloprotease (MMP) cleavage site of collagen type I and functions as a specific proteolysis target for several MMPs, namely MMP1 and 2,[28] with predicted cleavage between the Gly and Ile residues.[29,30] The C-terminal sequence was the integrin-dependent cell adhesion motif Arg-Gly-Asp-Ser (RGDS) found in several cell adhesion molecules and used extensively in biomaterial research, including similar PA systems,[31] to elicit cell attachment, promote survival, and control cell encapsulation and phenotype.[5]

The rationale behind our specific design was to create a defined supermolecular two-dimensional template able to promote cell attachment, instruct the attached cells to synthesize and deposit a tissue-specific ECM matrix, and ultimately degrade through specific protease activity endogenous to the newly formed tissue. Accordingly, it was shown that by controlling the cleavage of the PA, the native-like tissue was able to eliminate the adhesive properties of the original template without requiring additional protease supplementation to the medium, and consequently induce its self-release as a structurally intact live construct with potential downstream future applications.

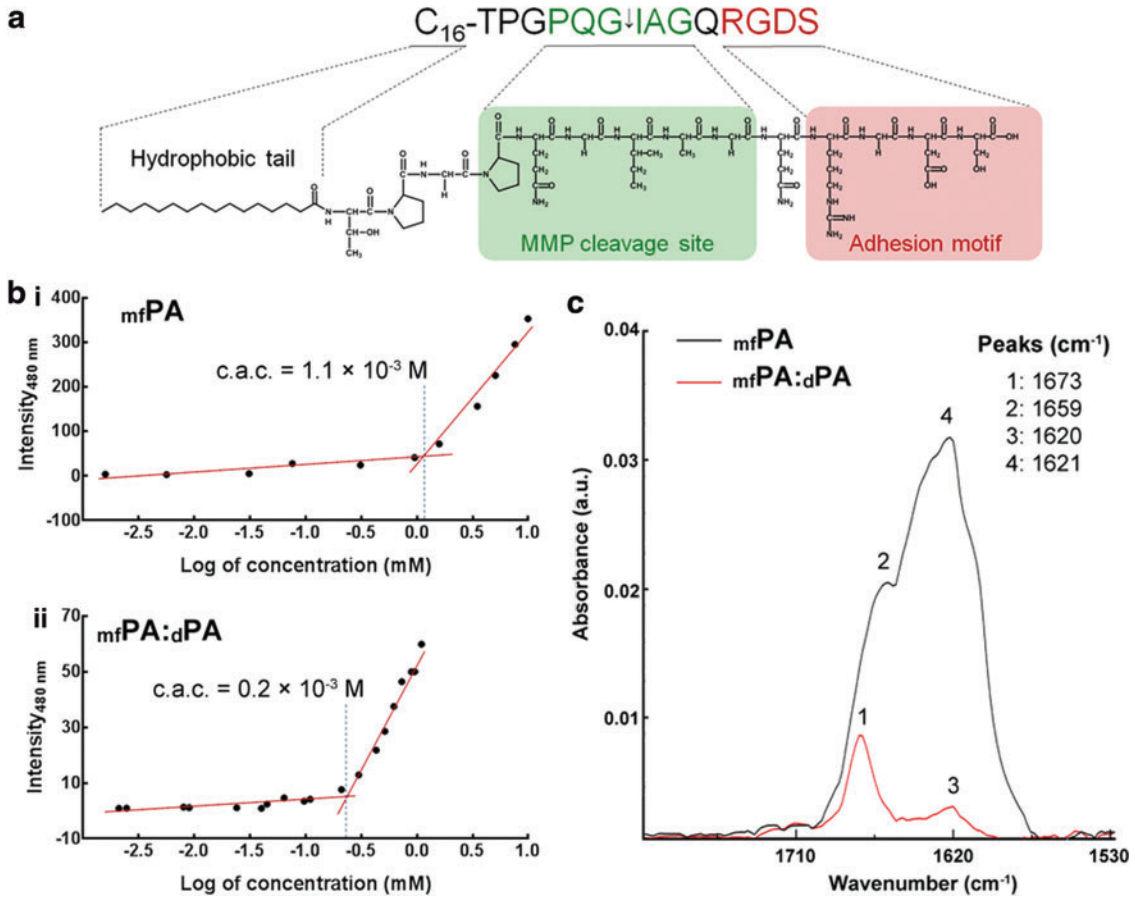

FIG. 1. The multifunctional C_{16}-TPGPQGIAGQRGDS peptide amphiphile ($_{mf}$PA). **(a)** Schematic structure of $_{mf}$PA comprising a hydrophobic C_{16} aliphatic chain linked to a hydrophilic 14 amino acid peptide formed by an enzyme-responsive sequence (in *green*; ↓ indicates the target site for matrix metalloprotease [MMP]-specific cleavage), followed by the integrin-binding RGDS motif (*red*). **(b)** Critical aggregation concentration (c.a.c.) of $_{mf}$PA in (i) single and (ii) binary systems mixed with diluent PA at a 15:85 mol/mol ratio ($_{mf}$PA:$_{d}$PA). **(c)** Fourier transform infrared (FTIR) spectroscopy analysis of $_{mf}$PA (*black*) and $_{mf}$PA:$_{d}$PA (*red*) with corresponding peaks. Color images available online at www.liebertpub.com/tea

Materials and Methods

Synthesis of PAs

PAs were custom synthesized by CS Bio as >95% pure trifluoroacetic acid salts and their molecular weight confirmed by electrospray mass spectrometry. Lyophilized C_{16}-TPGPQG↓IAGQRGDS ($_{mf}$PA; ↓ indicates cleavage site for MMP1) and C_{16}-ETTES ($_{d}$PA)[32] were weighed and dissolved as single or binary component solutions in ultrapure water from a Barnstead Nanopure system to the desired concentrations. For binary PA systems, $_{mf}$PA and $_{d}$PA were mixed in mol/mol ratios. The C_{16}-GGGRGDS ($_{sf}$PA),[24] C_{16}-TPGPQG, and IAGQRGDS molecules were similarly prepared as single component solutions.

Cell culture

Corneal tissues were obtained as by-products of grafting procedures and kindly provided by Mr. Martin Leyland, BSc, MD, FRCOphth, following informed consent. All experiments were approved by the Royal Berkshire NHS Foundation Trust (RBFT) R&D Office and in accordance with RBFT and MHRA ethics guidelines. Human corneal stromal fibroblasts (hCSFs) were isolated from epithelia-depleted corneal rings and cultured as previously described.[33] For additional details, see the Supplementary Materials and Methods section (Supplementary Data are available online at www.liebertpub.com/tea).

Preparation of PA coatings

To produce thin, dry film coatings, 100 μL aliquots from PA solutions at 1×10^{-5}–10^{-2} M were spotted as ≈ 1.5 cm^2 drops onto standard or low-attachment, tissue culture plastic surfaces (Nunc) and left to dry overnight at room temperature inside an aseptic, Class II cell culture cabinet. Resulting films were washed thrice with sterile phosphate-buffered saline (PBS) just before cell seeding. Stability of PA coatings was assessed by imaging film coatings upon drying (day 0) and after incubation in serum-free medium (SFM) at 37°C for 7 days using a LumaScope inverted light microscope (Etaluma). Conditioned medium enriched with endogenous MMPs (cSFM) was prepared by incubating confluent hCSFs with SFM for 5 days immediately before use in stability assays. MMP-free conditioned medium ($_{RA}$SFM) was similarly produced while adding 1×10^{-5} M of all-*trans* retinoic acid (RA; Sigma-Aldrich) every other day to inhibit hCSFs from expressing MMPs.[33]

Adhesion and proliferation assays

To evaluate the biocompatibility and bioactivity of $_{mf}$PA, single and binary PA coatings were produced on low-attachment, tissue culture plastic surfaces and then seeded with 1.5×10^{4} hCSFs·cm^{-2} in serum-free culture medium supplemented with 1×10^{-5} M RA. Cell adhesion and proliferation were evaluated using the AlamarBlue assay (Life Technologies) according to the manufacturer's instructions (see the Supplementary Materials and Methods section). Water-treated polystyrene surfaces were used as uncoated control. To assess adhesion specificity, hCSFs were incubated for 30 min with 5×10^{-5} M of $_{d}$PA (mock), $_{sf}$PA, anti-αVβ5 integrin antibody (ab24694; Abcam), or cyclo [Arg-Gly-Asp(D-Phe)-NMe-Val] (cRGD; CS Bio) before seeding, and the cell number was evaluated 24 h postseeding. All experiments were performed in triplicate.

Analysis of gene marker expression

Cells seeded at 1.5×10^{4} hCSFs·cm^{-2} on 1.25 mM $_{mf}$PA:$_{d}$PA at a 15:85 mol/mol ratio or $_{d}$PA templates coating normal cell culture plates were grown for 21 days in serum-free culture medium supplemented with 1×10^{-5} M RA, and then harvested for mRNA isolation by standard Trizol extraction (Life Technologies) and evaluation of gene expression as previously described[27,33] (see the Supplementary Materials and Methods section).

Biofabrication and self-release of 3D tissue

Coatings produced on low-attachment cell culture plates using 1.25 mM $_{mf}$PA:$_{d}$PA at 15:85 mol/mol served as templates for adhesion, proliferation, and stratification of hCSFs. Cells were seeded (5×10^{4} cells·cm^{-2}) and cultured for 90 days in SFM + 1×10^{-5} M RA to allow the fabrication of an ECM-rich tissue, and then maintained in non-supplemented SFM for 3 days to elicit MMP expression and consequent tissue self-release. Tissue detachment was monitored by following removal of RA from the culture medium by time-lapse bright-field microscopy using a remote-operated LumaScope inverted microscope inside the tissue incubator.

Reattachment assays

Self-released tissues (R1) were sampled using a reusable 3-mm Harris micropunch (Sigma-Aldrich) and then reconditioned in RA-supplemented SFM for 3 days to suppress MMP expression endogenous to the tissue. Reconditioned tissues were then transferred to new uncoated or $_{mf}$PA:$_{d}$PA-coated low-attachment plates and maintained in RA-supplemented SFM. A glass coverslip was used to hold the tissue plane in close contact with the surface. After 7 days, glass coverslips were removed and tissues were washed with PBS and imaged from above and diagonally using a Pentax Optio 750Z digital camera (Pentax). Tissues attached to the $_{mf}$PA:$_{d}$PA coating were then released as before by removal of RA from the culture medium. These second-time self-released tissues (R2) were again sampled, and the re-attachment/redetachment process repeated for a third time (R3). Samples were used immediately after punching to evaluate cell viability using the Live/Dead Cell double staining kit (CalBioChem; Merck) according to the manufacturer's instructions. Calcein- and propidium iodide-stained cells were imaged using an Axio Imager fluorescence microscope (Zeiss) at λ_{em} = 515 and 620 nm, respectively. Quantification of total viable cells was performed by analyzing 10 different fields per sample from 3 independent samples.

Contraction assays

Free-floating self-released tissues, R1, R2, and R3, were imaged (day 0) using a Nikon D90 digital camera (Nikon) and then incubated in cell culture medium containing 5% fetal bovine serum (FBS) to elicit myofibroblast differentiation of hCSFs. After 7 days, tissues were again imaged

(day 7) and contraction evaluated by calculating the ratio between the initial and final areas for each tissue using the ImageJ v1.46 software.

Statistical analysis

Error bars represent the standard deviation of the mean, analyzed *a priori* for homogeneity of variance. Replicates from each independent experiment were confirmed to follow a Gaussian distribution, and differences between groups were determined using one- or two-way analysis of variance, followed by Bonferroni's multiple comparison *post hoc* test. Significance between groups was established for $p < 0.05$, 0.01, and 0.001, with a 95% confidence interval, and R^2 values of 0.7585, 07591, 0.9031, 0.9291, and 0.9814 for the proliferation, gene expression, contraction, viability, and MMP1 expression assays, respectively.

Results and Discussion

Biophysical characterization of the PAs

The $_{mf}$PA was solubilized from lyophilized powder in ultrapure water and its critical aggregation concentration (c.a.c.) determined by Thioflavin T (ThT) fluorescence was 1.1×10^{-3} M (Fig. 1b, upper panel). Fourier transform infrared (FTIR) spectroscopy experiments above the c.a.c. showed that $_{mf}$PA self-assembled with a secondary β-sheet structure, as is denoted by the positive band at $1620\,cm^{-1}$ (Fig. 1c), suggesting its arrangement into highly organized structures.[24] This was supported by transmission electron microscopy (TEM), which showed that $_{mf}$PA forms well-defined polydisperse nanotapes, 528 ± 83 Å wide (Fig. 2a), displaying 5.6 ± 0.8 Å-thick stripes along the main axis of the fiber (Fig. 2a, left inset), expectedly associated with the internal lamellar structure of the nanotapes.[24]

The sensitivity of $_{mf}$PA (*m/z* 1578.87) to specific cleavage by metalloproteases was analyzed by mass spectrometry after incubation of $_{mf}$PA nanotapes with MMP1. This enzyme specifically recognized the cleavage sequence designed for $_{mf}$PA, producing the expected peptide fragment, IAGQRGDS, detected at *m/z* 803.43 (Fig. 2b). A smaller moiety corresponding to the GQRGDS peptide was also detected at *m/z* 619.3, indicating some residual proteolytic cleavage or degradation. However, the cleavage product, C_{16}-TPGPQG, was not detected by mass spectrometry. This product self-assembled above 8.6×10^{-5} M (Supplementary Fig. S1) and formed micelle-like structures (Supplementary Fig. S2) similar to those observed in MMP1-treated $_{mf}$PA (Fig. 2b). In contrast, no self-assembly was detected for the IAGQRGDS peptide (Supplementary Fig. S1). These results suggested that, upon cleavage of the $_{mf}$PA by MMP1, the RGDS-containing peptide is released into the medium, whereas the newly formed C_{16}-TPGPQG fragment remained assembled within the pre-existing nanotapes, forming distinct self-assembling structures. The specificity of cleavage was further tested by incubating $_{mf}$PA with proteolysis buffer only or with recombinant MMP7. MMP7 was previously shown to be expressed by various cell types, including hCSFs,[34] but unable to target the MMP-cleavage sequence included in the $_{mf}$PA.[29,35] No cleavage products were obtained after these treatments (Fig. 2b), demonstrating that the cleavable motif of the $_{mf}$PA is recognized only by specific proteases.

Several studies have shown that the bioactivity of PAs containing cell adhesion motifs can be augmented using

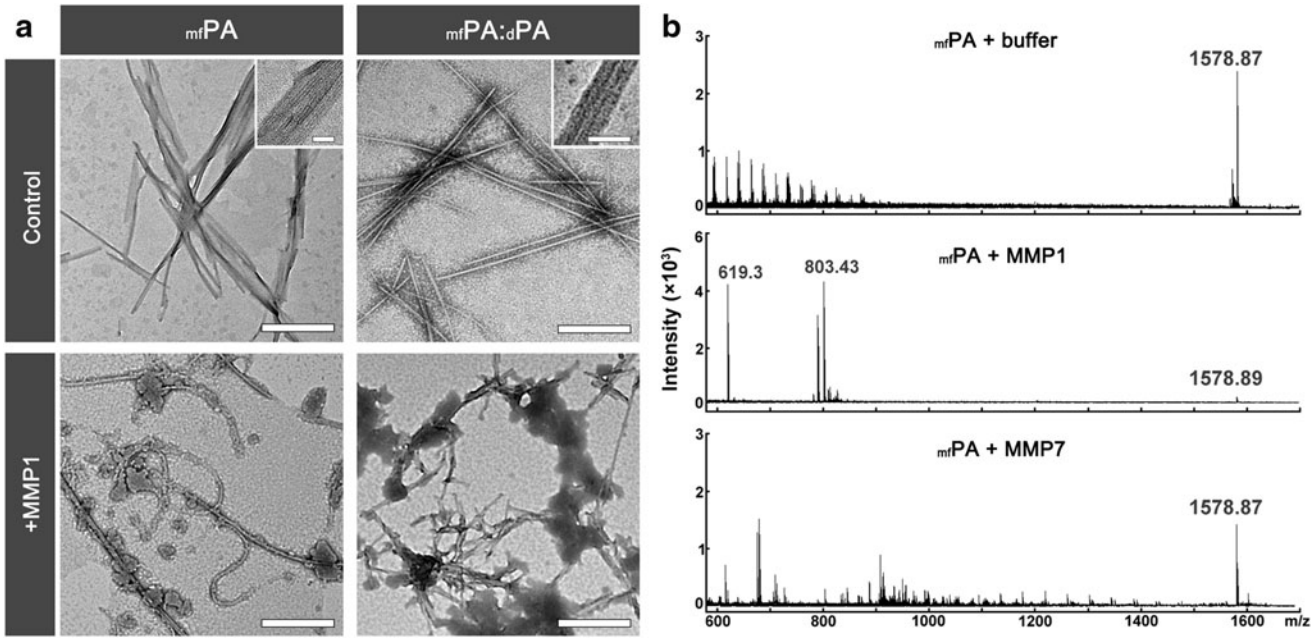

FIG. 2. Specific degradation of $_{mf}$PA by MMP1. **(a)** Transmission electron micrographs of self-assembled structures comprising $_{mf}$PA and $_{mf}$PA:$_{d}$PA. In aqueous solution, these PA systems formed well-defined polydisperse nanotapes (control) that degrade when treated with a protease able to recognize the enzyme-responsive sequence of $_{mf}$PA (+MMP1). Scale bars, 500 nm (*insets*, 50 nm). **(b)** Enzyme-catalyzed cleavage of $_{mf}$PA in solution. The products of the reaction with enzymes that cleave (+MMP1) or are unable to recognize the enzyme-responsive sequence of $_{mf}$PA (+MMP7) were analyzed by mass spectrometry and compared with enzyme-free control (+buffer).

diluent PA molecules to space the bioactive molecules in the assembled nanostructure,[27,36] thus creating binary PA systems that minimize interaction between bioactive motifs.[32] Recently, we have used the nonbioactive, negatively charged C_{16}-Glu-Thr-Thr-Glu-Ser molecule (hereby designated $_{d}$PA) as such a diluent to achieve the optimal cell adhesion activity of an RGDS-containing PA.[27] Similarly, we produced a binary PA system by combining $_{mf}$PA with $_{d}$PA in water. ThT fluorescence analysis showed that the c.a.c. of the mixed system was five times lower than single-system $_{mf}$PA (Fig. 1b), indicating that the aggregation process was driven by the $_{d}$PA, probably due to its higher degree of hydrophobicity. FTIR for $_{mf}$PA:$_{d}$PA denoted a β-sheet secondary structure with a positive band at $1620\,cm^{-1}$ (Fig. 1c). The existence of a single c.a.c. for the binary $_{mf}$PA:$_{d}$PA system suggested an interaction between $_{mf}$PA and $_{d}$PA molecules. Additional evidence was found by TEM, where the self-assembly of the mixed binary system led to the formation of nanotapes, 254 ± 41 Å wide (Fig. 2a), displaying stripes similar to those observed for single-system $_{mf}$PA (Fig. 2a, right inset). Furthermore, these nanotapes were also sensitive to cleavage by the proteolytic activity of MMP1 (Fig. 2a, bottom right panel). Altogether, these results indicate that $_{mf}$PA:$_{d}$PA coassembled and formed homogeneous nanostructures where the bioactive enzyme-responsive $_{mf}$PA is interspersed with $_{d}$PA molecules.

Bioactivity of the PA templates

The bioactivity of single and mixed PA systems was tested by evaluating the potential of $_{mf}$PA and $_{mf}$PA:$_{d}$PA to promote integrin-dependent cell attachment and direct cell phenotype. For that, various concentrations of PAs in solution were drop-spotted and dry-coated onto low-attachment cell culture plates, allowing the formation of thin film coatings (Fig. 3). The stability of these films was tested after incubation with SFM previously conditioned by hCSFs (cSFM, containing secreted MMPs). As controls, MMP-free media, that is, fresh SFM or medium conditioned in the presence of all-*trans* RA ($_{RA}$SFM), were used. RA is a metabolite of vitamin A that suppresses MMP expression while enhancing ECM production from various cell types, namely hCSFs[33] and skin fibroblasts.[37] The results demonstrated that, after 7 days in cSFM, $_{mf}$PA and $_{mf}$PA:$_{d}$PA films were partially removed with considerable fraying and degradation of the edges (Fig. 3, cSFM). In contrast, when incubated with MMP-free media (Fig. 3, SFM or $_{RA}$SFM), the films remained intact and comparable as before incubation (Fig. 3, day 0). This effect was shown to be specific to films containing the $_{mf}$PA molecule as films comprising a single function PA, $_{sf}$PA (i.e., with the RGDS motif, but without the MMP-cleavable sequence[27]), were not degraded in cSFM (Fig. 3). These results further suggested that the supplementation of cell culture medium with RA constituted a simple and reliable method to control the cleavage of $_{mf}$PA, and consequently, to regulate the ability of $_{mf}$PA-containing coatings to provide a template for cell attachment. Moreover, the use of RA as a medium supplement was physiologically relevant as this metabolite has been shown to play a fundamental role in the correct development, function, and regeneration of many organs,[38] as well as in cancer prevention.[39] As such, RA was supplemented to SFM in subsequent cell culture experiments, unless otherwise noted.

The optimal bioactivity of the film coatings was assessed for $_{mf}$PA mixed with $_{d}$PA in ratios from 0:100 ($_{d}$PA only) to 100:0 mol/mol ($_{mf}$PA only) and at final concentrations of

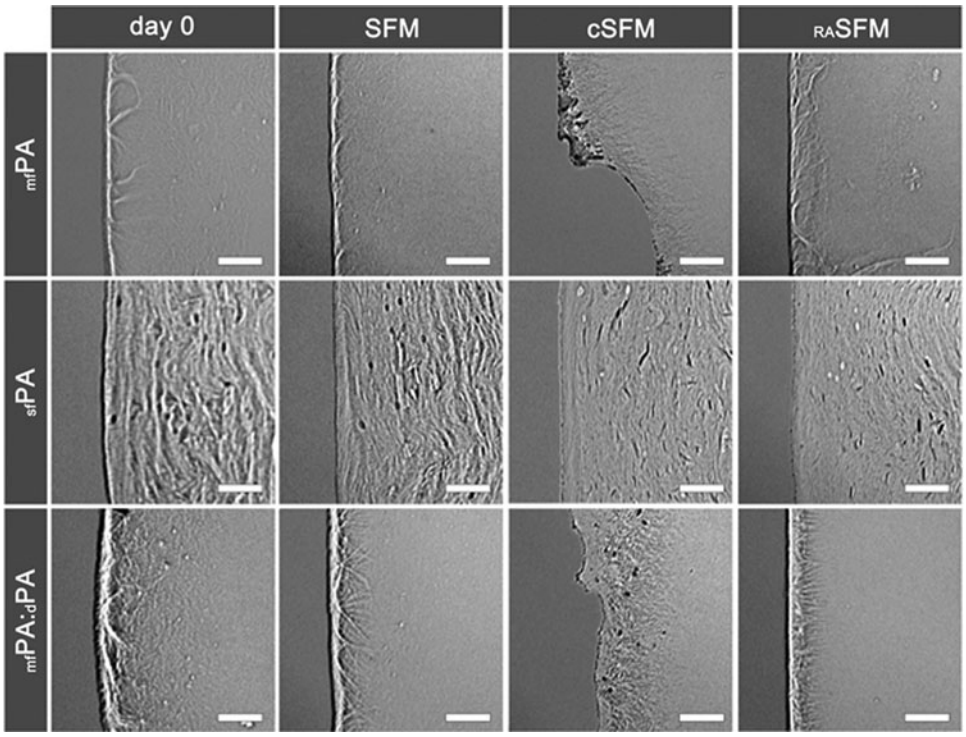

FIG. 3. Stability of PA coatings. Self-assembled $_{mf}$PA and $_{mf}$PA:$_{d}$PA structures dry-coated on cell culture surfaces produced continuous films (day 0) that degraded after incubation with conditioned culture medium (cSFM), but remained stable in MMP-free media (serum-free medium [SFM] or $_{RA}$SFM). This effect was specific to $_{mf}$PA-containing coatings and not to functional PAs without an MMP-responsive sequence ($_{sf}$PA). Scale bars, 20 μm.

1×10^{-5}–10^{-2} M. The activity of the different PA coatings was assessed by counting the number of attached hCSFs after 7 days in culture. Low-attachment plates were used as the underlying culture surface to minimize cell adhesion on uncoated areas. The results showed that all coatings containing $_{mf}$PA were able to support cell adhesion and proliferation, whereas $_{d}$PA coatings (0:100 ratio) and uncoated controls were not (Fig. 4). Cells grown on biofunctional adhesive coatings assumed an extended fibroblast-type morphology similar to that presented by cells attached to standard polystyrene culture surfaces, but those on $_{d}$PA remained round shaped (Fig. 4a). The adhesive activity of the coatings was shown to be dependent on $_{mf}$PA concentration up to 1.25×10^{-3} M and on the PA ratio, with an optimum at 15:85 mol/mol $_{mf}$PA:$_{d}$PA. Furthermore, these coatings were shown to bind cells specifically and dependently on αVβ3 integrins (Supplementary Fig. S3). PA coatings above 1.25×10^{-3} M were shown to be toxic to the cells attached in the early stage of culture, inducing cell death and consequent detachment (Fig. 4b). Thus, we hypothesize that the optimal bioactivity found for the 15:85 mol/mol ratio resulted from a balance between the highest epitope density and the lowest epitope crowding effect. Moreover, the susceptibility to degradation by MMPs observed for this binary PA system in solution (Fig. 2) and as a coating (Fig. 3) was not due to the presence of the $_{d}$PA as coatings produced solely from $_{d}$PA were stable in cSFM (Supplementary Fig. S4). As such, to maximize the interaction between the surface coating and cells, all further experiments were performed using the 15:85 mol/mol $_{mf}$PA:$_{d}$PA binary system.

Integrin-mediated cell adhesion has been shown to modulate gene and protein expression and control cell phenotype.[40] Previous studies have shown that, when cultured in serum-free media, hCSFs revert to a characteristic alpha smooth muscle actin (αSMA)-negative phenotype and express a defined panel of markers that include keratocan, lumican, decorin, and aldehyde dehydrogenase A1 (ALDH1), all of which are fundamental for the function of the native tissue.[41,42] In this context, the effect of $_{mf}$PA:$_{d}$PA coating on the expression of several hCSF gene markers was evaluated

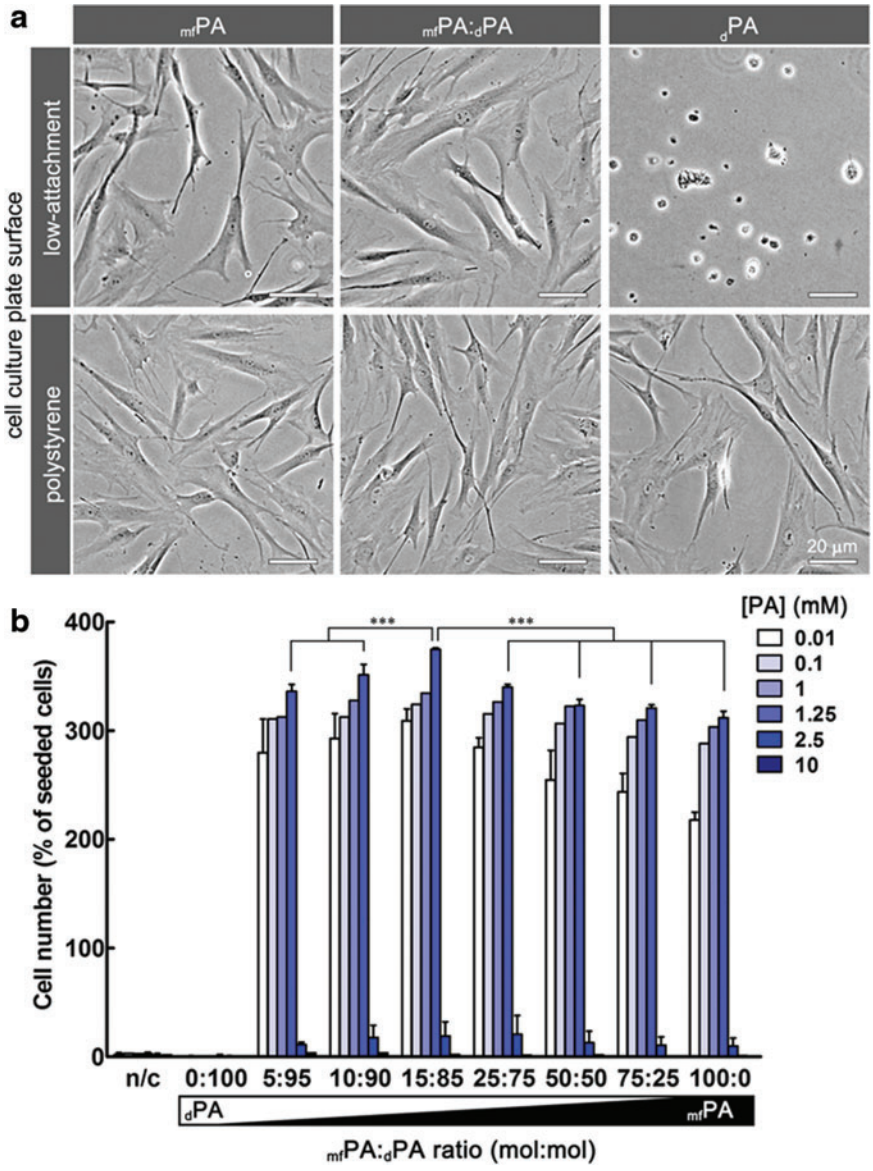

FIG. 4. The adhesive and proliferative bioactivity of $_{mf}$PA. **(a)** The adhesive properties of $_{mf}$PA and $_{mf}$PA:$_{d}$PA coatings allowed human corneal stromal fibroblasts (hCSFs) to attach on low-attachment cell culture plates (*upper panels*) as in normal culture polystyrene surfaces (*lower panels*). This effect was dependent on the RGDS motif of $_{mf}$PA and not observed in nonbioactive $_{d}$PA coatings. Scale bars, 20 μm. **(b)** Effect of concentration and the $_{mf}$PA:$_{d}$PA dilution ratio on hCSF proliferation. Cells grown on PA films coating low-attachment surfaces were counted after 7 days in culture. Proliferation increased with increasing PA concentration up to 1.25 mM, after which PA coatings induced cell death. In all viable coatings, maximum proliferative effect was observed for $_{mf}$PA:$_{d}$PA at the 15:85 mol/mol ratio. No attachment was observed in noncoated (n/c) or $_{d}$PA-coated surfaces (0:100 ratio). Data are expressed as average ± standard deviation (SD) of three independent experiments ($n=3$); *** corresponded to $p<0.001$. Color images available online at www.liebertpub.com/tea

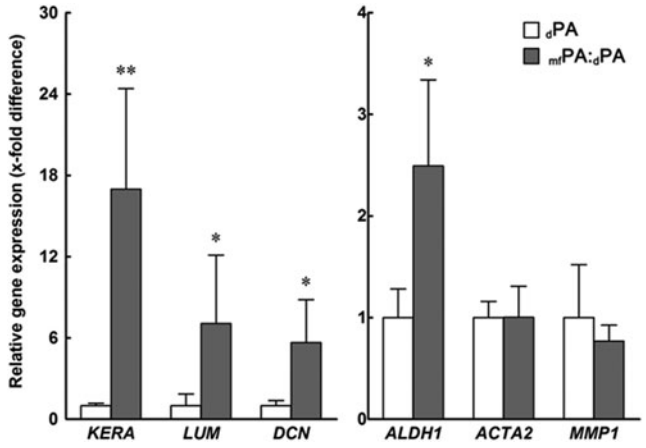

FIG. 5. Effect of $_{mf}$PA on the molecular phenotype of hCSFs. Relative expression of genes coding for hCSF-characteristic extracellular matrix (ECM) components (*KERA*, *LUM*, *DCN*, and *ALDH1*) was significantly increased in cells grown for 21 days on $_{mf}$PA:$_{d}$PA (*grey*) when compared with $_{d}$PA coatings (*white bars*). Data are expressed as average ± SD of three independent experiments ($n = 3$); * and ** corresponded to $p < 0.05$ and 0.01, respectively.

by reverse transcription quantitative–polymerase chain reaction and compared with that of cells on $_{d}$PA-coated and uncoated surfaces (Fig. 5). In this particular assay, normal cell culture polystyrene plates were used to allow cells to adhere and grow, irrespectively of the coating. Importantly, hCSFs grown on bioactive $_{mf}$PA:$_{d}$PA coatings showed significant upregulation for genes coding for keratocan, lumican, decorin, and ALDH1 (*KERA*, *LUM*, *DCN*, and *ALDH1*, respectively) compared with cells on nonbioactive $_{d}$PA coatings (Fig. 5). However, no effect was observed in the transcription levels of *ACTA2* (the gene coding for αSMA, a marker of myofibroblastic differentiation[43]) or *MMP1* (Fig. 5). Furthermore, no differences in gene expression were observed between cells grown on $_{d}$PA-coated and uncoated surfaces (data not shown). Together, these results showed that the bioactive PA not only promoted cell adhesion but also directed cell phenotype by enhancing the expression of several specific ECM components without compromising the proven MMP repression effect from RA supplementation to cultured hCSFs.[33]

Controlled degradation of PA template and tissue self-release

The potential of $_{mf}$PA:$_{d}$PA to act as a template capable of inducing the formation of self-releasable tissues under physiological conditions was tested by coating it onto low-attachment culture plates. These plates were subsequently used for the adhesion and long-term culture of hCSFs in serum-free RA-supplemented medium (Fig. 6a). Under these conditions, cells were able to attach, proliferate, and survive for 90 days (Fig. 6b and c) without compromising the adhesive PA surface. The combined effects from $_{mf}$PA:$_{d}$PA interaction and RA signaling[33] ensured that cells proliferated up to day 60 (Fig. 6b and c, d60) and stratified from day 30 onward, creating a multilayered construct comprising a cell-derived dense tissue within the boundaries of the PA template (Fig. 6b, d30–d90). Concomitantly, cells maintained in RA-supplemented medium suppressed MMP expression, with corresponding culture supernatants presenting MMP activities below 5% of that from nonsupplemented conditioned medium (Fig. 7). As such, newly formed tissue was cumulatively deposited by cells, and no visible degradation was observed for the entire 90-day period of culture (Fig. 6b). After 90 days in culture, the PA-instructed hCSFs were able to fabricate structurally representative corneal tissue, with an interwoven matrix comprising densely packed collagen fibers and associated native-type proteoglycans, such as keratocan, lumican, and decorin (Fig. 8). These proteoglycans only partially colocalized with the collagen fibers, also occupying the space between the collagenous matrix and the cell layers (Fig. 8, blue staining; also Supplementary Figs S5–S7).

Upon formation of the biofabricated constructs at day 90, tissue cultures were then maintained in the medium without RA (Fig. 6a), and MMP proteolytic activity was monitored each day for 3 days (days +1, +2, and +3). Removal of RA supplementation resulted in a cumulative increase of proteolytic activity in the culture supernatant over time (Fig. 7), a consequence of MMPs being expressed from cells within the tissue constructs. Although MMP activity at day +3 corresponded to only 45% ± 13% of that from conditioned medium, it allowed the newly formed tissues to completely detach from the surface of the culture plate and emerge (Fig. 6a and Supplementary Video S1). This indicated that, by day +3, the MMP activity accumulated in the medium was sufficient to cleave the RGDS motif from the $_{mf}$PA:$_{d}$PA nanotapes and degrade the adhesive coating template (Fig. 6a). The subsequent self-release and liftoff of the tissue at day +3 resulted in a small, but significant, loss of cells (Fig. 6c). However, the free-floating construct maintained its structural integrity (Fig. 9 and Supplementary Video S2), with no apparent loss of the dense ECM present at d90 (Fig. 6b, +3).

Similarly, skin fibroblasts seeded onto the PA surface templates and cultured for 90 days in RA-supplemented SFM were able to attach, proliferate, and fabricate ECM-dense three-dimensional tissues. Following the same method of RA removal, the newly formed skin tissues were able to express endogenous MMPs, thus degrading the adhesive PA template and promoting their self-detachment while retaining structural integrity and shape (Supplementary Video S3). These results indicated that more than one cell type can be applied to this PA system and to produce easily recoverable structurally intact tissues through the physiologically relevant RA supplementation/removal mechanism. However, for cell types where RA is not a feasible regulator of endogenous MMP expression, alternative systems could be used with predictably similar results. For example, alternative inhibitors of MMP expression (such as the anticancer agents Marimastat,[44] Ro 28-2653,[45] and doxycycline[46]) or enzymatic activity (e.g., tissue inhibitors of metalloproteinase or α_2-macroglobulin[47]) could be added throughout the culture process, and then removed to transiently increase MMP activity and elicit the degradation of the PA template and tissue release.

Functional characterization of self-released tissue equivalents

To further characterize the efficacy of the self-release process, the viability, ultrastructure, and function of the

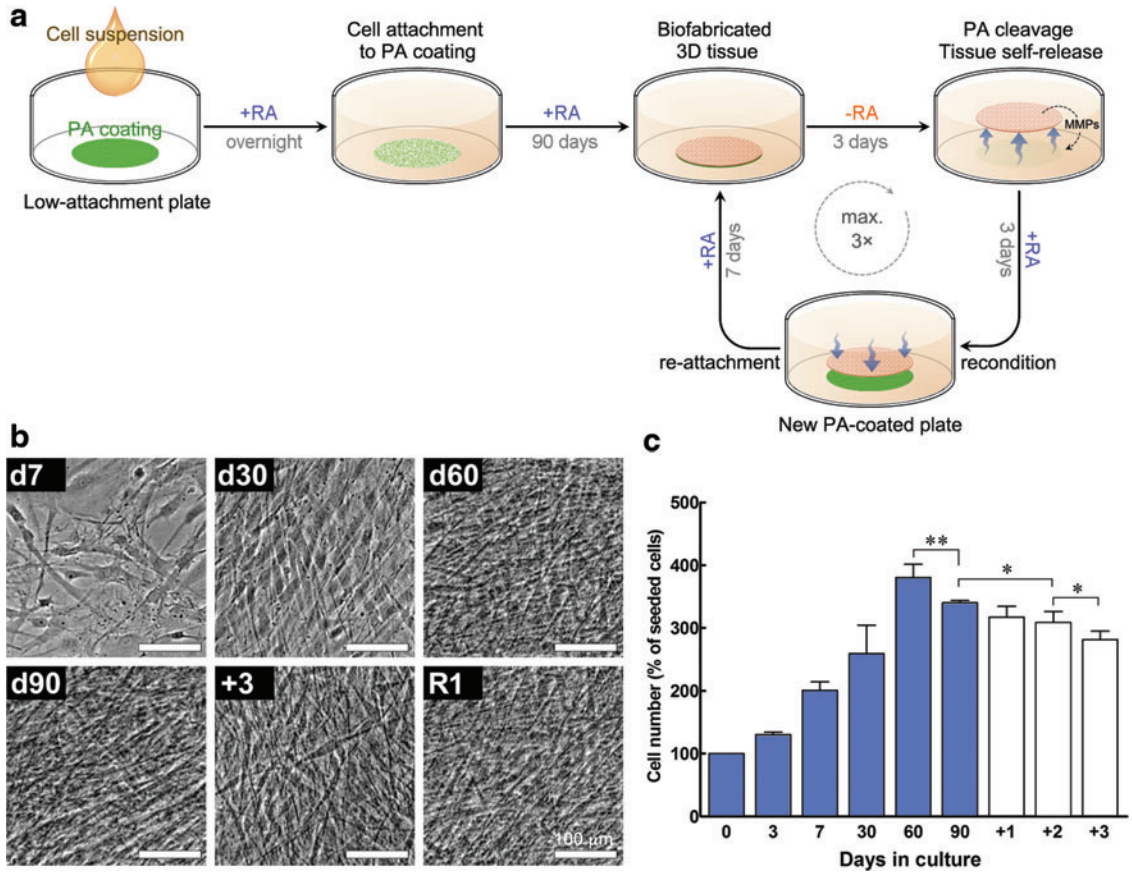

FIG. 6. Proof of concept for the use of $_{mf}$PA as a template to induce the biofabrication and control the self-release of tissues by donor-derived cells. **(a)** Schematic diagram depicting how cells isolated from human donors were seeded and grown on low-attachment plates coated with 1.25 mM $_{mf}$PA:$_{d}$PA at the 15:85 mol/mol ratio (*green*) in retinoic acid (RA)-supplemented SFM (*blue*). Tissues fabricated in the course of the 90-day culture period were induced to express MMPs into the culture supernatant after RA removal from the medium (*orange*), thus providing the cue to degrade the adhesive PA coating and induce their self-release (*blue arrows*). Lifted tissues were then easily recoverable for downstream applications, namely for thrice-repeated reattachment and relifting processes, using only RA-induced regulation of endogenous MMP expression. **(b)** Phase-contrast micrographs of hCSFs growing as a monolayer on $_{mf}$PA:$_{d}$PA templates (day [d]7) and integrating the tissue formed by PA-induced ECM deposition and accumulation before (d30–d90), during (+3), and after tissue self-release (R1). Scale bars, 100 µm. **(c)** Proliferation of hCSFs grown on $_{mf}$PA:$_{d}$PA templates. Cell proliferation in RA-containing SFM (*blue bars*) increased up to day 60, and then decreased at day 90 and in the following 3 days, when incubated in SFM without RA (*white bars*, +1, +2, and +3). Data are expressed as average ± SD of three independent experiments ($n = 3$); * and ** corresponded to $p < 0.05$ and 0.01, respectively. Color images available online at www.liebertpub.com/tea

self-lifted tissues were analyzed. Tissue function and viability were tested by determining the capacity of the corneal stromal constructs to reattach to an adhesive surface after MMP-induced self-release while maintaining their constituent cells alive. For this, first-time self-released tissues (R1) were punch-sampled to assess cell viability through a live/dead cell assay, reconditioned in RA-containing medium for 3 days to suppress MMP expression, and then transferred to a new $_{mf}$PA:$_{d}$PA-coated, low-attachment cell culture plate for reattachment (Fig. 6a). After 7 days, tissue constructs were shown to be planar and strongly attached to $_{mf}$PA:$_{d}$PA-coated surfaces (Fig. 10a, R1), but not to uncoated controls where they remained free-floating (Fig. 10a, uncoated). Furthermore, the viability of cells comprising the tissue was maintained with 92% ± 1% of live cells (Fig. 10b and c, R1). The ultrastructure of R1 corneal stromal tissues was evaluated by TEM (Fig. 10d). These 10.1 ± 1.8-µm-thick bioconstructs comprised two or three cells layers separated by 2.6 ± 1.6-µm-thick regions of ECM (Fig. 10d, upper panel) characterized by densely packed collagen fibrils with an average diameter of 27.6 ± 2.8 nm and a *d*-spacing of 58.5 ± 4.5 nm (Fig. 10d, lower panels). Interestingly, the ECM thickness of these tissues was similar to that of stromal lamellae (i.e., the building blocks) of native human corneas.[48] Moreover, the calculated diameter and *d*-spacing parameters were comparable with those of collagen type I fibers found in the human cornea,[48,49] representing an improvement over similar tissue constructs produced *de novo* by diverse methods.[50,51] These results were consistent with those obtained by confocal immunofluorescence microscopy (Fig. 8) and constituted proof that the tissue fabric produced *in vitro* by hCSFs grown in $_{mf}$PA:$_{d}$PA-coated surfaces was remarkably similar to that of the native corneal stroma.

The endurance of the tissue constructs was further tested by repeating the relift, punching, and reattachment processes two additional times, consecutively (Fig. 6a). Second-time

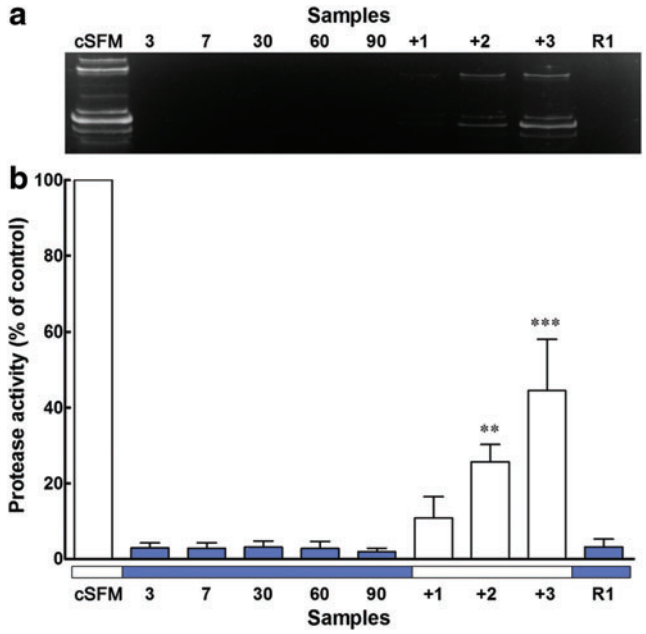

FIG. 7. MMP activity from cell culture supernatants. **(a)** Representative casein gel zymogram and **(b)** corresponding densitometry analysis of supernatant samples collected from 5-day conditioned medium (cSFM) and from various time points where cells were cultured with (*blue*) or without RA (*white bars*). Data are expressed as average ± SD of three independent experiments ($n = 3$); ** and *** corresponded to $p < 0.01$ and 0.001, respectively. Color images available online at www.liebertpub.com/tea

released tissues (R2) were always able to reattach to coated surfaces while maintaining shape throughout the manipulation process (Fig. 10a). In addition, cell viability remained high with R2 tissues maintaining 85% ± 13% of live cells (Fig. 10b, c), representing maintenance of cell viability

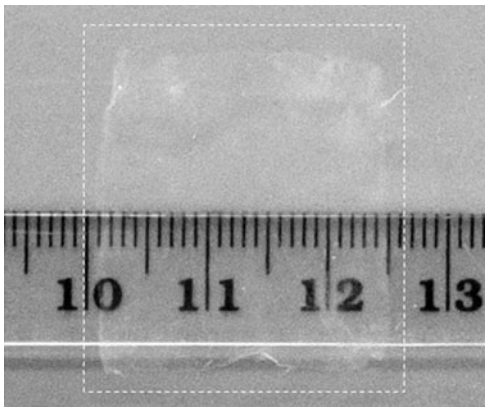

FIG. 9. Photograph of free-floating, human corneal tissue fabricated by hSCFs. Tissue constructs fabricated by cells during 90 days recovered their ability to express MMPs after being maintained in SFM without RA. The endogenous MMPs expressed by the tissue were capable of degrading the underlying $_{mf}$PA:$_{d}$PA template after 3 days, thus inducing the tissue self-release from its adhesive bottom surface without any external manipulation. The resulting free-floating tissue was transparent in water and retained its original shape and structural integrity. A decimal ruler was used as scale.

within the tissue for 13 days following initial release (Fig. 6a). Reattachment was even observed after three consecutive self-releases (Fig. 10a, R3), despite evidence of some structural damage and a significant reduction in cell viability to 40% ± 2% (Fig. 10c). These results demonstrate that the fabricated tissue constructs were very robust, being able to respond to RA deprivation, control their MMP-mediated self-release, and then be RA reconditioned and reattach to an adhesive surface three consecutive times. In addition, tissues remained structurally whole and morphologically intact despite their thickness and the endogenous MMPs

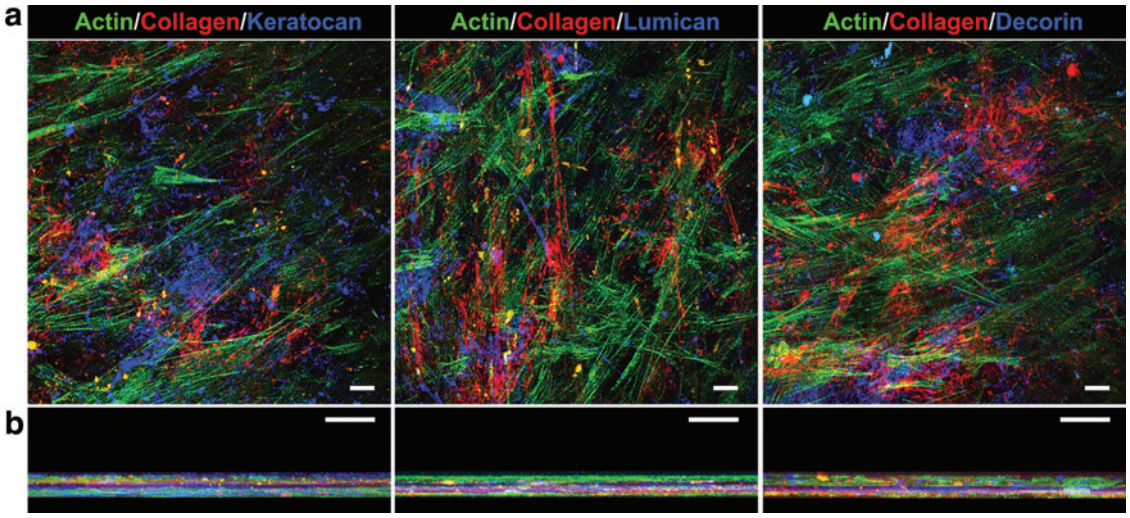

FIG. 8. Immunofluorescence confocal microscopy of self-detached tissue constructs. **(a)** Representative *top* view and **(b)** *z*-stack view of corneal tissues fabricated by hCSFs grown on $_{mf}$PA:$_{d}$PA templates for 90 days. Tissue constructs showed that they comprise multiple layers of collagen type I fibers (*red*) deposited between actin-stained cells (*green*) and form an ECM enriched with hCSF-characteristic proteoglycans (*blue*), such as keratocan (*left*), lumican (*center*), and decorin (*right panels*). Scale bars, 20 μm. Color images available online at www.liebertpub.com/tea

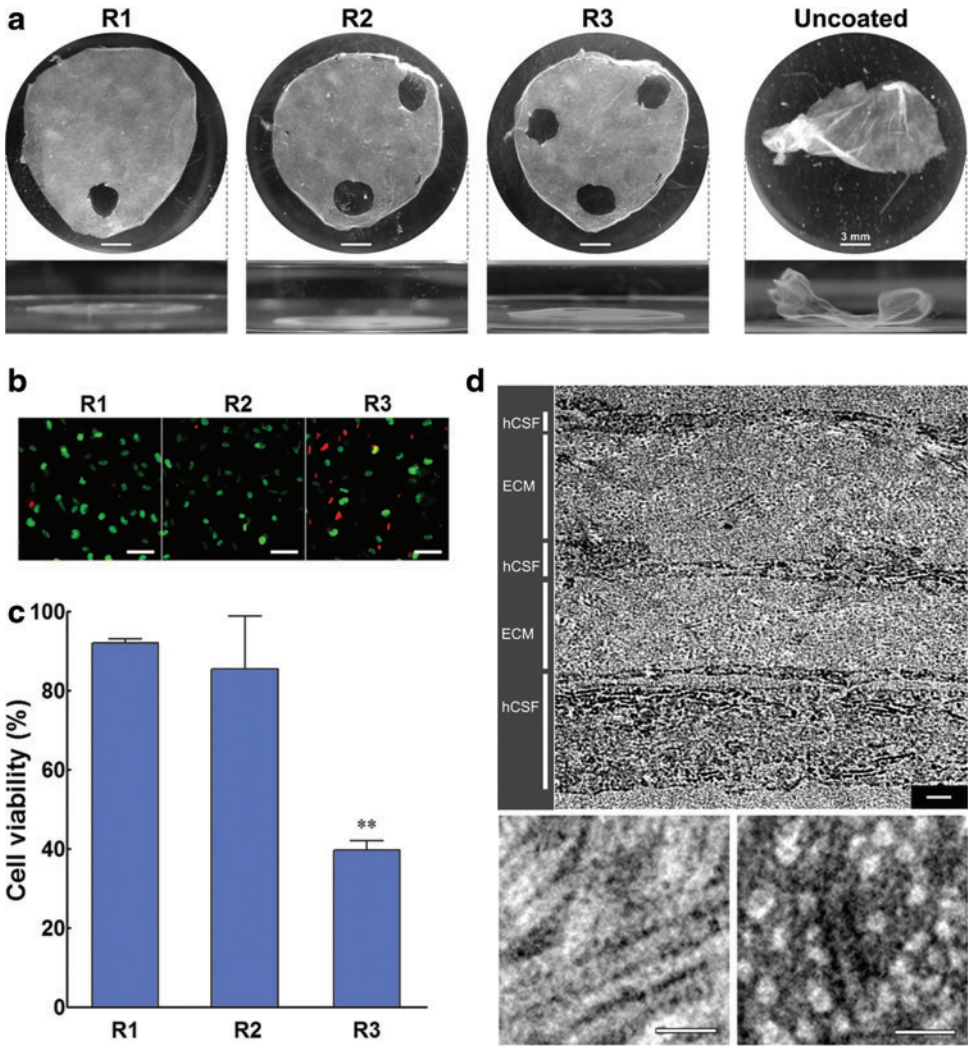

FIG. 10. Macro-, micro-, and ultrastructural stability of tissues fabricated and self-released from PA templates. **(a)** Reattachment of biofabricated tissues after one (R1), two (R2), or three consecutive self-detachments (R3) to low-attachment plates with or without (uncoated) $_{mf}$PA:$_{d}$PA. Self-released tissues were punch-sampled and reconditioned in RA-supplemented SFM before being transferred for reattachment (Fig. 6a). Scale bars, 3 mm. **(b)** Live and dead hCSFs integrating the self-released tissues imaged by fluorescence microscopy using calcein (*green*)/propidium iodide (*red*) cell staining (Scale bars, 20 μm), and **(c)** corresponding cell viability was calculated for R1, R2, and R3 tissue constructs. Data are expressed as average ± SD of three independent experiments ($n = 3$); ** corresponded to $p < 0.01$. **(d)** Ultrastructure of R1 was observed by transmission electron microscopy, evidencing the multilayered organization of the tissue (*upper panel*), with intercalating layers of hCSFs and deposited ECM comprising densely packed collagen fibrils (*lower panels*). Scale bars, 500 nm (*upper*), 100 nm (*lower panels*). Color images available online at www.liebertpub.com/tea

eliciting tissue self-release. These results also suggested that self-released tissue constructs could perform well as live transplantable equivalents. Cell sheet constructs used as corneal,[52] esophageal,[53] tracheal,[54] myocardial,[55] and hepatic[56] implants have previously shown improved practical and functional advantage due to their intrinsic ability to attach to the recipient organ without the need for sutures or carrier materials, leading to quicker graft integration and organ regeneration.[57] As such, the demonstrated ability of the self-released tissues to reattach to adhesive surfaces represents a promising clinical application.

The specific function of cells within the released tissues was also evaluated. It is known that hCSFs play a fundamental role in response to corneal injury *in vivo* by assuming a contractile myofibroblastic phenotype.[43] This cellular function was simulated here by exposing free-floating, corneal stromal tissues after self-release to FBS for 7 days (Fig. 11a). The results showed that R1 tissues contracted to 8% ± 3% of their initial area (Fig. 11b), indicating that cells comprising the tissue constructs were activated and contractile. The hCSFs comprising second- (R2) and third-time self-released tissues (R3) were also prone to activation, as demonstrated by tissue contraction to a corresponding 9% ± 5% and 32% ± 5% of their initial size (Fig. 11). The reduced contraction from R3 could be explained by the lower number of resident hCSFs within those tissues (Fig. 10c). However, the cells remaining alive were still capable of performing a change in phenotype and activating into myofibroblasts. Together, these results showed that tissue fabricated *in vitro* by hCSFs grown on $_{mf}$PA:$_{d}$PA templates were structurally and functionally similar to native stromal tissue from human corneas and that the controlled self-release resulting from the specific degradation of the adhesive $_{mf}$PA:$_{d}$PA coating allowed an easy tissue recovery (Supplementary Video S2) with minimal damage to its cells or ECM structure. Furthermore, even after extensive manipulation, the tissues were able to reattach and relift three consecutive times while remaining functionally active for an additional 26-day period in culture, as demonstrated by the contraction assay.

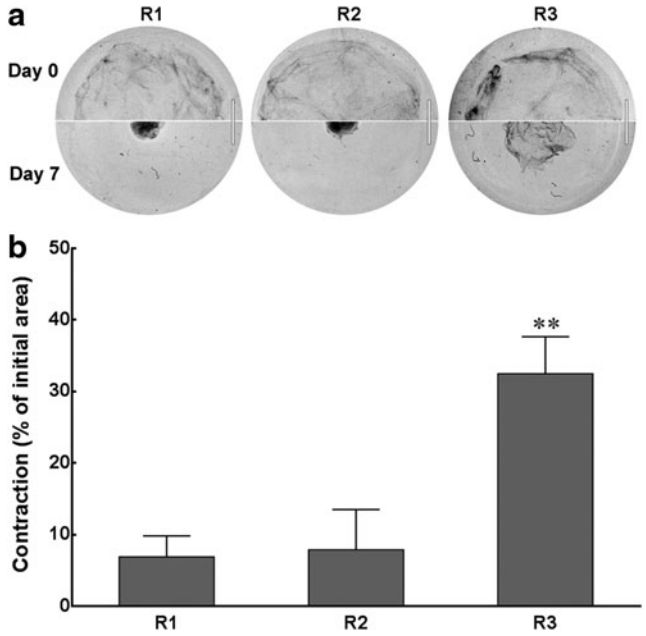

FIG. 11. Biofunctional performance of tissues fabricated and self-released from PA templates. Myofibroblastic activity of hCSFs from self-released R1, R2, and R3 tissues after incubation in fetal bovine serum (FBS)-containing medium. **(a)** Representative photographs taken before (day 0, *upper half*) and after FBS incubation (day 7, *lower half*) were overlapped to evidence reduction in the tissue area. Scale bars, 5 mm. **(b)** Quantification of tissue contraction expressed as a ratio between the final and initial areas of tissue. Data are expressed as average ± SD of three independent experiments ($n = 3$); ** corresponded to $p < 0.01$.

Conclusions

In light of our results, we postulate that the use of multifunctional PA templates constitutes a promising strategy to fabricate native-like tissue sheets *in vitro*. First, the $_{mf}$PA is a simple molecule that spontaneously self-assembles in aqueous medium in single or binary systems at relatively low concentrations. Second, the resulting nanostructures produced stable biofunctional templates by dry coating, a quick, simple, and highly transferable method. Third, PA nanostructures can be assembled from multiple molecules. Thus, it is reasonable to assume that more than one biofunctional PA can be added to the system to create a more complex template, that is, one that can fine-tune cell behavior through consecutive or sequential activation of multiple signaling pathways. The potential of multicomponent PAs is well demonstrated in our $_{mf}$PA:$_{d}$PA templates, where the diluent $_{d}$PA molecule significantly increased the bioactivity of the RGDS motif. Through this motif, $_{mf}$PA:$_{d}$PA coatings were able to instruct cells isolated from human donors to fabricate native-like corneal or skin bioconstructs while simultaneously controlling tissue adhesion to the surface. As release occurs through degradation of the coating PA, no external carrier is present upon tissue recovery, nor is it required due to the tissues' intrinsic robustness. The ability to retain shape and reattach represents a promising feature for tissue/organ engineering[58] and grafting,[57] making these biofabricated constructs suitable for transplantation applications. Individual constructs can also be folded or stacked to increase tissue thickness and evaluate its optical properties (i.e., transparency).

Overall, these properties make the $_{mf}$PA a highly transferable versatile material that, pending future comparative studies, can represent a physiologically integrated alternative to other scaffold-free bottom-up strategies used to create tissues *in vitro*.[59] As such, this smart material will provide a plausible platform for the biofabrication of certain tissues to source autologous transplantation. Furthermore, due to the material's ability to proceed under physiological conditions, we envision its use in the creation of new implantable medical devices for cell therapy applications, both capable of directing the growth and subsequent release of therapeutic cells/tissues within locations known to have varying MMP levels, such as in developing tumors or during wound healing.

Acknowledgments

The authors thank for P. Harris and M. Spink from EM-Lab for their technical expertise and support with electron microscopy and T. Gibson from CAF, University of Reading, for his support with mass spectrometry analysis and data processing. This work was funded by the BBSRC (grant reference BB/I008187/1).

Disclosure Statement

No competing financial interests exist.

References

1. Griffith, L.G., and Swartz, M.A. Capturing complex 3D tissue physiology in vitro. Nat Rev Mol Cell Bio **7,** 211, 2006.
2. Lutolf, M.P., Gilbert, P.M., and Blau, H.M. Designing materials to direct stem-cell fate. Nature **462,** 433, 2009.
3. Rice, J.J., Martino, M.M., De Laporte, L., Tortelli, F., Briquez, P.S., and Hubbell, J.A. Engineering the regenerative microenvironment with biomaterials. Adv Health Mater **2,** 57, 2013.
4. Berthiaume, F., Maguire, T.J., and Yarmush, M.L. Tissue engineering and regenerative medicine: history, progress, and challenges. Annu Rev Chem Biomol **2,** 403, 2011.
5. Place, E.S., Evans, N.D., and Stevens, M.M. Complexity in biomaterials for tissue engineering. Nat Mater **8,** 457, 2009.
6. Seliktar, D. Designing cell-compatible hydrogels for biomedical applications. Science **336,** 1124, 2012.
7. Mosiewicz, K.A., Kolb, L., van der Vlies, A.J., Martino, M.M., Lienemann, P.S., Hubbell, J.A., Ehrbar, M., and Lutolf, M.P. In situ cell manipulation through enzymatic hydrogel photopatterning. Nat Mater **12,** 1071, 2013.
8. Samchenko, Y., Ulberg, Z., and Korotych, O. Multipurpose smart hydrogel systems. Adv Colloid Interface Sci **168,** 247, 2011.
9. Dixon, J.E., Shah, D.A., Rogers, C., Hall, S., Weston, N., Parmenter, C.D.J., McNally, D., Denning, C., and Shakesheff, K.M. Combined hydrogels that switch human pluripotent stem cells from self-renewal to differentiation. Proc Natl Acad Sci U S A **111,** 5580, 2014.
10. Kharkar, P.M., Kiick, K.L., and Kloxin, A.M. Designing degradable hydrogels for orthogonal control of cell microenvironments. Chem Soc Rev **42,** 7335, 2013.

11. Mager, M.D., LaPointe, V., and Stevens, M.M. Exploring and exploiting chemistry at the cell surface. Nat Chem **3,** 582, 2011.
12. Sanchez, C., Arribart, H., and Guille, M.M.G. Biomimetism and bioinspiration as tools for the design of innovative materials and systems. Nat Mater **4,** 277, 2005.
13. Boekhoven, J., and Stupp, S.I. 25th anniversary article: supramolecular materials for regenerative medicine. Adv Mater **26,** 1642, 2014.
14. Hamley, I.W. Self-assembly of amphiphilic peptides. Soft Matter **7,** 4122, 2011.
15. Zhang, S.G. Fabrication of novel biomaterials through molecular self-assembly. Nat Biotechnol **21,** 1171, 2003.
16. Hartgerink, J.D., Beniash, E., and Stupp, S.I. Peptide-amphiphile nanofibers: a versatile scaffold for the preparation of self-assembling materials. Proc Natl Acad Sci U S A **99**, 5133, 2002.
17. Stupp, S.I., Zha, R.H., Palmer, L.C., Cui, H.G., and Bitton, R. Self-assembly of biomolecular soft matter. Faraday Discuss **166,** 9, 2013.
18. Zhao, X.B., Pan, F., Xu, H., Yaseen, M., Shan, H.H., Hauser, C.A.E., Zhang, S.G., and Lu, J.R. Molecular self-assembly and applications of designer peptide amphiphiles. Chem Soc Rev **39,** 3480, 2010.
19. Wu, E.C., Zhang, S.G., and Hauser, C.A.E. Self-assembling peptides as cell-interactive scaffolds. Adv Funct Mater **22,** 456, 2012.
20. Liu, J.S., and Gartner, Z.J. Directing the assembly of spatially organized multicomponent tissues from the bottom up. Trends Cell Biol **22,** 683, 2012.
21. Patel, N.G., and Zhang, G. Responsive systems for cell sheet detachment. Organogenesis **9,** 93, 2013.
22. Kelm, J.M., and Fussenegger, M. Scaffold-free cell delivery for use in regenerative medicine. Adv Drug Deliv Rev **62,** 753, 2010.
23. Yamato, M., Akiyama, Y., Kobayashi, J., Yang, J., Kikuchi, A., and Okano, T. Temperature-responsive cell culture surfaces for regenerative medicine with cell sheet engineering. Prog Polym Sci **32,** 1123, 2007.
24. Castelletto, V., Gouveia, R.M., Connon, C.J., and Hamley, I.W. New RGD-peptide amphiphile mixtures containing a negatively charged diluent. Faraday Discuss **166,** 381, 2013.
25. Castelletto, V., Gouveia, R.M., Connon, C.J., Hamley, I.W., Seitsonen, J., Nykanen, A., and Ruokolainen, J. Alanine-rich amphiphilic peptide containing the RGD cell adhesion motif: a coating material for human fibroblast attachment and culture. Biomater Sci **2,** 362, 2014.
26. Jones, R.R., Castelletto, V., Connon, C.J., and Hamley, I.W. Collagen stimulating effect of peptide amphiphile C-16-KTTKS on human fibroblasts. Mol Pharm **10,** 1063, 2013.
27. Gouveia, R.M., Castelletto, V., Alcock, S.G., Hamley, I.W., and Connon, C.J. Bioactive films produced from self-assembling peptide amphiphiles as versatile substrates for tuning cell adhesion and tissue architecture in serum-free conditions. J Mater Chem B **1,** 6157, 2013.
28. Patterson, J., and Hubbell, J.A. Enhanced proteolytic degradation of molecularly engineered PEG hydrogels in response to MMP-1 and MMP-2. Biomaterials **31,** 7836, 2010.
29. Billinghurst, R.C., Dahlberg, L., Ionescu, M., Reiner, A., Bourne, R., Rorabeck, C., Mitchell, P., Hambor, J., Diekmann, O., Tschesche, H., Chen, J., VanWart, H., and Poole, A.R. Enhanced cleavage of type II collagen by collagenases in osteoarthritic articular cartilage. J Clin Invest **99,** 1534, 1997.
30. Turk, B.E., Huang, L.L., Piro, E.T., and Cantley, L.C. Determination of protease cleavage site motifs using mixture-based oriented peptide libraries. Nat Biotechnol **19,** 661, 2001.
31. Jun, H.W., Yuwono, V., Paramonov, S.E., and Hartgerink, J.D. Enzyme-mediated degradation of peptide-amphiphile nanofiber networks. Adv Mater **17,** 2612, 2005.
32. Hamley, I.W., Dehsorkhi, A., and Castelletto, V. Coassembly in binary mixtures of peptide amphiphiles containing oppositely charged residues. Langmuir **29,** 5050, 2013.
33. Gouveia, R.M., and Connon, C.J. The effects of retinoic acid on human corneal stromal keratocytes cultured in vitro under serum-free conditions. Invest Ophthalmol Vis Sci **54,** 7483, 2013.
34. Sivak, J.M., and Fini, M.E. MMPs in the eye: emerging roles for matrix metalloproteinases in ocular physiology. Prog Retin Eye Res **21,** 1, 2002.
35. Imai, K., Hiramatsu, A., Fukushima, D., Pierschbacher, M.D., and Okada, Y. Degradation of decorin by matrix metalloproteinases: identification of the cleavage sites, kinetic analyses and transforming growth factor-beta 1 release. Biochem J **322,** 809, 1997.
36. Webber, M.J., Tongers, J., Renault, M.A., Roncalli, J.G., Losordo, D.W., and Stupp, S.I. Development of bioactive peptide amphiphiles for therapeutic cell delivery. Acta Biomater **6,** 3, 2010.
37. Fisher, G.J., and Voorhees, J.J. Molecular mechanisms of photoaging and its prevention by retinoic acid: ultraviolet irradiation induces MAP kinase signal transduction cascades that induce Ap-1-regulated matrix metalloproteinases that degrade human skin in vivo. J Investig Dermatol Symp Proc **3,** 61, 1998.
38. Rhinn, M., and Dolle, P. Retinoic acid signalling during development. Development **139,** 843, 2012.
39. Tang, X.H., and Gudas, L.J. Retinoids, retinoic acid receptors, and cancer. Annu Rev Pathol **6,** 345, 2011.
40. Hynes, R.O. Integrins: bidirectional, allosteric signaling machines. Cell **110,** 673, 2002.
41. Jester, J.V., Moller-Pedersen, T., Huang, J.Y., Sax, C.M., Kays, W.T., Cavangh, H.D., Petroll, W.M., and Piatigorsky, J. The cellular basis of corneal transparency: evidence for 'corneal crystallins'. J Cell Sci **112,** 613, 1999.
42. Kao, W.W.Y., and Liu, C.Y. Roles of lumican and keratocan on corneal transparency. Glycoconj J **19,** 275, 2002.
43. Funderburgh, J.L., Mann, M.M., and Funderburgh, M.L. Keratocyte phenotype mediates proteoglycan structure: a role for fibroblasts in corneal fibrosis. J Biol Chem **278,** 45629, 2003.
44. Rasmussen, H.S., and McCann, P.P. Matrix metalloproteinase inhibition as a novel anticancer strategy: a review with special focus on batimastat and marimastat. Pharmacol Ther **75,** 69, 1997.
45. Lein, M., Jung, K., Ortel, B., Stephan, C., Rothaug, W., Juchem, R., Johannsen, M., Deger, S., Schnorr, D., Loening, S., and Krell, H.W. The new synthetic matrix metalloproteinase inhibitor (Roche 28-2653) reduces tumor growth and prolongs survival in a prostate cancer standard rat model. Oncogene **21,** 2089, 2002.
46. Liu, J., Xiong, W.F., Baca-Regen, L., Nagase, H., and Baxter, B.T. Mechanism of inhibition of matrix metalloproteinase-2 expression by doxycycline in human aortic smooth muscle cells. J Vasc Surg **38,** 1376, 2003.

47. Visse, R., and Nagase, H. Matrix metalloproteinases and tissue inhibitors of metalloproteinases: structure, function, and biochemistry. Circ Res **92,** 827, 2003.
48. Komai, Y., and Ushiki, T. The three-dimensional organization of collagen fibrils in the human cornea and sclera. Invest Ophthalmol Vis Sci **32,** 2244, 1991.
49. Holmes, D.F., Gilpin, C.J., Baldock, C., Ziese, U., Koster, A.J., and Kadler, K.E. Corneal collagen fibril structure in three dimensions: structural insights into fibril assembly, mechanical properties, and tissue organization. Proc Natl Acad Sci U S A **98,** 7307, 2001.
50. Wu, J., Du, Y.Q., Watkins, S.C., Funderburgh, J.L., and Wagner, W.R. The engineering of organized human corneal tissue through the spatial guidance of corneal stromal stem cells. Biomaterials **33,** 1343, 2012.
51. Wu, J., Rnjak-Kovacina, J., Du, Y.Q., Funderburgh, M.L., Kaplan, D.L., and Funderburgh, J.L. Corneal stromal bioequivalents secreted on patterned silk substrates. Biomaterials **35,** 3744, 2014.
52. Nishida, K., Yamato, M., Hayashida, Y., Watanabe, K., Yamamoto, K., Adachi, E., Nagai, S., Kikuchi, A., Maeda, N., Watanabe, H., Okano, T., and Tano, Y. Corneal reconstruction with tissue-engineered cell sheets composed of autologous oral mucosal epithelium. N Engl J Med **351,** 1187, 2004.
53. Ohki, T., Yamato, M., Murakami, D., Takagi, R., Yang, J., Namiki, H., Okano, T., and Takasaki, K. Treatment of oesophageal ulcerations using endoscopic transplantation of tissue-engineered autologous oral mucosal epithelial cell sheets in a canine model. Gut **55,** 1704, 2006.
54. Kanzaki, M., Yamato, M., Hatakeyama, H., Kohno, C., Yang, J., Umemoto, T., Kikuchi, A., Okano, T., and Onuki, T. Tissue engineered epithelial cell sheets for the creation of a bioartificial trachea. Tissue Eng **12,** 1275, 2006.
55. Miyahara, Y., Nagaya, N., Kataoka, M., Yanagawa, B., Tanaka, K., Hao, H., Ishino, K., Ishida, H., Shimizu, T., Kangawa, K., Sano, S., Okano, T., Kitamura, S., and Mori, H. Monolayered mesenchymal stem cells repair scarred myocardium after myocardial infarction. Nat Med **12,** 459, 2006.
56. Ohashi, K., Yokoyama, T., Yamato, M., Kuge, H., Kanehiro, H., Tsutsumi, M., Amanuma, T., Iwata, H., Yang, J., Okano, T., and Nakajima, Y. Engineering functional two- and three-dimensional liver systems in vivo using hepatic tissue sheets. Nat Med **13,** 880, 2007.
57. Yang, J., Yamato, M., Shimizu, T., Sekine, H., Ohashi, K., Kanzaki, M., Ohki, T., Nishida, K., and Okano, T. Reconstruction of functional tissues with cell sheet engineering. Biomaterials **28,** 5033, 2007.
58. Haraguchi, Y., Shimizu, T., Sasagawa, T., Sekine, H., Sakaguchi, K., Kikuchi, T., Sekine, W., Sekiya, S., Yamato, M., Umezu, M., and Okano, T. Fabrication of functional three-dimensional tissues by stacking cell sheets in vitro. Nat Protoc **7,** 850, 2012.
59. Nagase, K., Kobayashi, J., and Okano, T. Temperature-responsive intelligent interfaces for biomolecular separation and cell sheet engineering. J R Soc Interface **6,** S293, 2009.

Address correspondence to:
Che John Connon, PhD
Institute of Genetic Medicine
Newcastle University
International Centre for Life
Central Parkway
Newcastle upon Tyne NE1 3BZ
United Kingdom

E-mail: che.connon@newcastle.ac.uk

Received: December 5, 2014
Accepted: February 17, 2015
Online Publication Date: March 24, 2015